2-Rényi CCNR Negativity of Compact Boson for multiple disjoint intervals

Himanshu Gaur

Department of Physics, Indian Institute of Technology Bombay, Powai, Mumbai, Maharashtra 400076 India

E-mail: 194123018@iitb.ac.in

ABSTRACT: We investigate mixed-state bipartite entanglement between multiple disjoint intervals using the computable cross-norm criterion (CCNR). We consider entanglement between a single interval and the union of remaining disjoint intervals, and compute 2-Rényi CCNR negativity for 2d massless compact boson. The expression for 2-Rényi CCNR negativity is given in terms of cross-ratios and Riemann period matrices of Riemann surfaces involved in the calculation. In general, the Riemann surfaces involved in the calculation of n-Rényi CCNR negativity do not possess a Z_n symmetry. We also evaluate the Reflected Rényi entropy related to the 2-Rényi CCNR negativity. This Reflected Rényi entropy is a universal quantity. We extend these calculations to the 2d massless Dirac fermions as well. Finally, the analytical results are checked against the numerical evaluations in the tight-binding model and are found to be in good agreement.

Contents

1 Introduction

Entanglement has been a driving force behind some of the recent developments in many frontiers of physics. Specifically entanglement has provided key insights in Gravity [1–3], Quantum computation [4], and Quantum many-body systems [5–8].

To study bipartite entanglement of a quantum system in pure states one often considers entanglement entropies, however, these measures fail to quantify entanglement in mixed states as they fail to distinguish between the classical and quantum correlations. Mutual Information fails to reliably detect entanglement as well since it suffers from similar issues. It is in general a hard problem to study entanglement for mixed states. One viable option is to consider separability criterion, in this regard PPT (Partial transpose) [9, 10] criterion has been often considered in quantum many-body systems. The computable cross norm (CCNR) [11, 12] is another such criterion considered recently in quantum many-body systems. In general, it is not known whether one criterion has an advantage over the other in detecting entanglement [13].

Entanglement has proven to be an indispensable tool in the study of critical systems [5], owing to its ability to detect the scaling of quantum correlations near the quantum

phase transitions [6–8, 14]. This has led to extensive research investigating entanglement in 2d Conformal Field Theories (CFTs). Entanglement studies in CFTs have been made in the context of critical systems [8, 15–21], non-equilibrium dynamics [17, 22–26], integrable models [27–33], and systems with boundaries or defects [34–42] with great success. Recently there has been a lot of interest in studying symmetry resolved entanglement in CFTs [43–56] as well.

Entanglement studies in CFTs involving disjoint interval settings have been particularly interesting. In this regard, mutual information was first considered in [57] to study entanglement between two disjoint intervals. Since then many studies have been made in similar settings. Entanglement of the disjoints intervals with its complement has been investigated by studying the Rényi entropies in [58–67]. To study entanglement between the disjoint intervals Rényi PPT negativities has been considered in [68–73]. One interesting aspect of entanglement in such studies is that the entanglement spectrum is not just sensitive to the central charge of the CFT but becomes sensitive to the local operator content of the CFT as well. However, these studies in general suffer a problem that it is not known how to analytically continue these results in the Rényi index from integer values to real values to obtain entanglement entropy and negativity. This is because the calculation of Rényi entropies requires evaluating partition functions on Riemann surfaces, and the genus of these surfaces varies with the Rényi index. It is worth mentioning here that these Riemann surfaces carry a Z_n symmetry, where n is the Rényi index. It was recently shown in [74], that when Rényi CCNR negativity for two disjoint intervals is considered, the Riemann surface involved in the calculations is always a torus of genus one. Hence these results can be analytically continued in Rényi index to find CCNR-negativity. The symmetry resolution of CCNR negativity has also been studied in quantum-many body systems [75, 76]. The Rényi CCNR negativities have also been shown to be related to the Reflected entropies, first introduced in the context of holography [77].

This work aims to extend the study of Rényi CCNR negativities to multiple disjoint intervals. When multiple-disjoint intervals are considered, the genus of the Riemann surfaces involved in the calculations of Rényi CCNR negativities again becomes sensitive to the Rényi index, however, a new feature is that these Riemann surfaces in general do not have Z_n symmetry. It is therefore interesting to study the features of CCNR-negativities in these settings. In the present work, we consider entanglement between a single interval, denoted A, and the rest of the disjoint intervals denoted B_i, see Figure 1 and compute the 2-Rényi negativity. We hope to generalise this result to arbitrary integer values of the Rényi index in future work. We will focus our attention on the compact boson CFT for our study.

The organisation of this work is as follows. In Section 2, we discuss the Rényi CCNR negativity and Reflected entropies. In Section 3, we review the replica trick and Twist fields used in the evaluation of the Rényi CCNR negativities. In section 4, we evaluate the 2-Rényi CCNR negativity, and the related Reflected entropy for compact boson and also extend these results to massless Dirac fermion. We also numerically check our results against the tight-binding model. Finally, in Section 5, we conclude the present work. We also have three appendices, containing necessary calculations, background material and
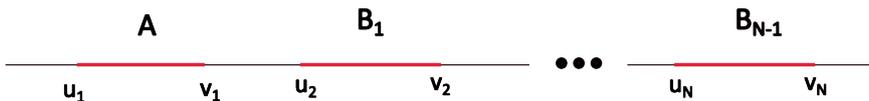
Figure 1.   Multiple Disjoint Intervals.   The interval A is (u_1, v_1) and the intervals B_i are (u_{i-1}, v_{i-1})

details of the numerical model used in the present study.

2   Computable Cross Norm Ratio

In this section, we will discuss the Rényi computable cross-norm negativity and Reflected Entropies. We consider a bipartite system composed of subsystems A, and B in a state ρ, where ρ can be a mixed-density matrix. Let us denote by $\{|a\rangle\}$, and $\{|b\rangle\}$ a complete set of basis on the Hilbert spaces $\mathcal{H}_A$ and $\mathcal{H}_B$, respectively. The key idea in computable cross norm negativity measures is to introduce the Re-alignment matrix R, given by

$$\langle a_1| \langle a_2| R |b_1\rangle |b_2\rangle = \langle a_1| \langle b_1| \rho |a_2\rangle |b_2\rangle. \tag{2.1}$$

A direct consequence of the Re-alignment is that R is not a square matrix. Consider the Singular Value decomposition (SVD) of $R = U\Sigma V^\dagger$, where Σ is a diagonal matrix, the Ky Fan norm or Computable cross norm (denoted CCNR or sometimes CCN) of R is then defined as $\text{Tr}(\Sigma)$. It is known that CCNR is a separability criterion, that is for separable density matrices ρ, the CCNR of the re-alignment matrix R is less than or equal to unity. It then follows that a CCNR of greater than unity means ρ is entangled, however just like the Partial Transpose Criterion(PPT) the converse is not necessarily true [11, 12]. To evaluate $\text{Tr}(\Sigma)$, let us consider the square matrix $RR^\dagger$, and define the Rényi CCNR entropy $\mathcal{E}_n$ as

$$\mathcal{E}_n = \log \text{Tr} \left(RR^\dagger \right)^n, \tag{2.2}$$

The CCNR-negativity is defined as the logarithm of the Computable Cross Norm of R, and is given by

$$\mathcal{E} = \lim_{n \to \frac{1}{2}} \mathcal{E}_n, \tag{2.3}$$

where $\mathcal{E}$ is just the logarithm of $\text{Tr}(\Sigma)$. It is known that Rényi CCNR entropy is closely related to Reflected entropy. Let us briefly discuss this relation, to introduce Reflected entropies, we consider the same settings. The idea is to introduce a purification $|\Omega\rangle$ of ρ^m. This is done using the Choi-Jamiolkowski isomorphism,

$$|\Omega_m\rangle = \frac{1}{\sqrt{\text{Tr}\rho^m}} \sum_{a_1,b_1,a_2,b_2} \langle a_1 b_1| \rho^{m/2} |a_2 b_2\rangle |a_1 b_1\rangle |a_2 b_2\rangle, \tag{2.4}$$

where the state $|\Omega_m\rangle$ belongs to the doubled Hilbert space $\mathcal{H}_A \otimes \mathcal{H}_B \otimes \mathcal{H}_A \otimes \mathcal{H}_B$. Reflected entropies study entanglement between the doubled subsystems AA and BB. The reflected reduced density matrix is

$$\rho_m(AA) = \text{Tr}_{BB} \left(|\Omega_m\rangle\langle\Omega_m| \right). \tag{2.5}$$

The Reflected Rényi entropies are then given by

$$S_{m,n}(AA) = \frac{1}{1-n} \log \mathrm{Tr} \rho_m^n(AA). \tag{2.6}$$

We see from eq.(2.1)-(2.2) that the Rényi CCNR negativity is just the un-normalised $m = 2$ Reflected Rényi entropy (upto a factor of $1 - n$),

$$S_{2,n}(AA) = \frac{1}{1-n} \mathcal{E}_n - \frac{n}{1-n} \log \left(\mathrm{Tr} \rho_{AA}^2 \right). \tag{2.7}$$

As we will see later, $S_{2,n}(AA)$ is a universal quantity in conformal field theory. Finally let us mention that generalisations of Rényi CCNR negativity, denoted (m, n)-Rényi CCNR negativities have been proposed in [75] which satisfy relations with Reflected entropies similar to eq.(2.7) for general values of m.

3 Replica Trick and Twist Fields

Let us start our discussion by considering the case of two intervals, as we will see that for this case the Replica geometry for the moments of $RR^\dagger$ is always a torus of genus one [74]. We will then end this section by setting the stage for the calculations in the case of multiple disjoint intervals. We will also see that the replica geometry in this case is not a torus with a fixed genus, but its genus increases with n.

We recall that the mixed density matrix ρ_{AB} for $A \cup B$ may be given in the field basis via the path integral on the single plane with cuts introduced along the intervals A, and B. The matrix product $RR^\dagger$ then amounts to taking two copies of ρ_{AB} and pasting them together along the cuts on B. The Riemann surface corresponding to $\mathrm{Tr} \left(RR^\dagger \right)^n$, is then constructed by taking the n copies of $RR^\dagger$ and pasting the cuts along A on the upper sheet of the jth copy with the cuts along A on the lower sheet of the $(j + 1)^{th}$ copy, where j runs over $\mathbb{Z} \mod n$. The resulting surface is shown in the Figure 2. It is not too difficult to see that this Riemann surface has a geometry of a genus-1 torus.

It is well known that for CFTs the evaluation of the partition function on the Riemann surface is equivalent to computing the correlation function of the Twist fields associated with this Riemann surface [27, 29]. The idea behind the Twist matrices is to consider the $n-$copies of the field on the plane and introduce Twist fields such that the monodromy of the fields around these Twist fields replicates the Replica trick construction of the Riemann surface. We have the following relation for the partition function Z_n

$$Z_n \propto \langle \mathcal{T}_{A,n}(u_1) \mathcal{T}_{A,n}(v_1) \mathcal{T}_{B,n}(u_2) \mathcal{T}_{B,n}(v_2) \rangle. \tag{3.1}$$

Since the Riemann surface consists of $2n$ sheets, we consider $2n$ copies of the field on the single sheet. These fields satisfy the following monodromy conditions around the Twist field,

$$\begin{aligned} \mathcal{T}_{A,n} &: 2j \leftrightarrow 2j + 1 \mod n, \\ \mathcal{T}_{B,n} &: 2j - 1 \leftrightarrow 2j \mod n, \end{aligned} \tag{3.2}$$
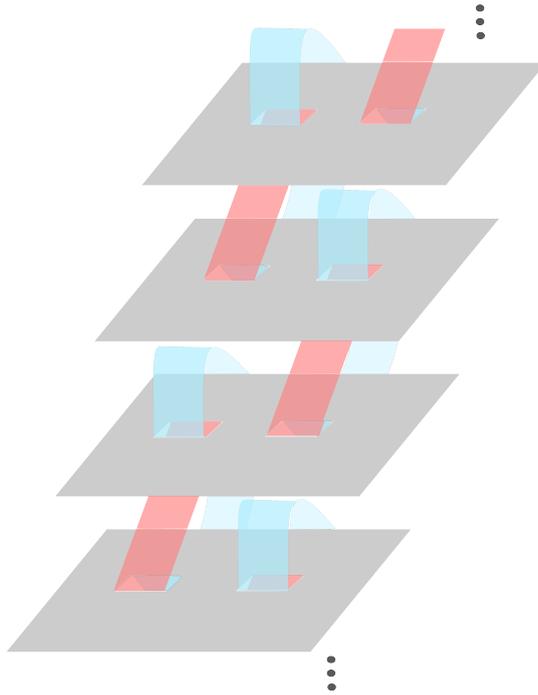
Figure 2. Riemann surface obtained for $\mathrm{Tr}\left(RR^{\dagger}\right)^n$ via the Replica trick.

where $j \in \{1, \cdots n\}$ and the field indices run over $\mathbb{Z} \mod 2n$. The scaling dimensions of these fields are $h_n = \frac{nc}{16}$, where c is the central charge of the CFT.

Now, the case of the multiple disjoint intervals may be similarly considered, here $RR^{\dagger}$ is constructed by joining the two copies of ρ_{AB} along $B = \cup_{i=1}^{N-1} B_i$, see Figure 1. The Riemann surface corresponding to n^{th} moment of $RR^{\dagger}$ is then similarly constructed. As mentioned at the start of this section, in this case however the genus of the resulting Riemann surface is not fixed, but it is given by $g = n(N-1) - (n-1)$. In this work, we will be interested in the $n = 2$ case only and the genus here will be $g = 2N - 3$. The partition function is again given by

$$Z_n \propto \langle \mathcal{T}_{A,n}(u_1)\mathcal{T}_{A,n}(v_1) \prod_{j=2}^{N} \mathcal{T}_{B,n}(u_j)\mathcal{T}_{B,n}(v_j)\rangle. \tag{3.3}$$

The major goal of this work is to compute this correlation function for $n = 2$ with an arbitrary number of intervals N in the theory of compact boson.

4   Compact Boson

Let us briefly introduce compact massless boson in $2d$. It is a conformally invariant theory with central charge $c = 1$. Its action is given by,

$$\mathcal{S} = \frac{1}{8\pi} \int \mathrm{d}^2x\, \partial_\mu\varphi\partial^\mu\varphi. \tag{4.1}$$

The target space of the field φ is compactified on a circle of radius R, that is we identify $\varphi \sim \varphi + 2\pi Rk$, where $k \in \mathbb{Z}$. Compact boson is the CFT of Luttinger liquids [78], and the compactification radius R is related to the Luttinger parameter K via the relation $K = \sqrt{2/R}$.

Let us recall the results for $n = 2$ Rényi entropy of multiple disjoint intervals, for two reasons, these results will be useful later, but more importantly to introduce some techniques that will be used later on. We, however, do not derive these expressions here but give necessary definitions and provide some of the technical details in the Appendix A. The partition function $\mathcal{Z}_{N,2}$ for the $n = 2$ Rényi Entropy is given by [60],

$$\mathcal{Z}_{N,2} = c_{N,2} \left| \frac{\prod_{j>i=1}^{N}(u_j - u_i)(v_j - v_i)}{\prod_{j,i=1}^{N}(v_i - u_j)} \right|^{\frac{1}{4}} \mathcal{F}(x_1, \cdots, x_{2N-3}), \tag{4.2}$$

where $c_{N,n}$ is a non-universal constant. The factor $\mathcal{F}$ is a function of the cross-ratios x_i, where

$$x_{2j-2} = \frac{(u_j - u_1)(v_N - u_N)}{(v_N - v_j)(u_N - u_1)}, \qquad x_{2j-1} = \frac{(v_j - u_1)(v_N - u_N)}{(v_N - v_j)(u_N - u_1)}, \tag{4.3}$$

with $j \in \{1, 2, \cdots N\}$ and it is given by

$$\mathcal{F}(x_1, \cdots, x_N) = \frac{\Theta(0|K\Pi)\,\Theta(0|\Pi/K)}{|\Theta(0|\Pi)|^2}. \tag{4.4}$$

In the above equation, Θ is the Riemann Siegel theta function. A $k-$dimensional theta function is defined as

$$\Theta \begin{bmatrix} \boldsymbol{\varepsilon} \\ \boldsymbol{\delta} \end{bmatrix} (\boldsymbol{\xi} \mid \Omega) \equiv \sum_{\boldsymbol{m} \in \mathbb{Z}^k} e^{i\pi(\boldsymbol{m}+\boldsymbol{\varepsilon})^t \cdot \Omega \cdot (\boldsymbol{m}+\boldsymbol{\varepsilon}) + 2\pi i (\boldsymbol{m}+\boldsymbol{\varepsilon})^t \cdot (\boldsymbol{\xi}+\boldsymbol{\delta})}, \tag{4.5}$$

where the characteristics $\boldsymbol{\varepsilon}$, $\boldsymbol{\delta} \in (\mathbb{Z}/2)^k$ and $\boldsymbol{\xi} \in \mathbb{C}^k$. In eq.(4.5), Ω is a $k \times k$ symmetric matrix with a positive definite imaginary part. For brevity the theta function in eq.(4.5) is denoted $\Theta(\boldsymbol{\xi}|\Omega)$ when $\varepsilon = \delta = 0$. In eq.(4.4), the $(N-1) \times (N-1)$ matrix Π is the Riemann period matrix of the Riemann surface $\tilde{\Sigma}_N$ parametrised by the algebraic curve

$$u^2 = \prod_{j=0}^{2N-2}(z - x_j), \tag{4.6}$$

see Appendix A for more details. This is just the Riemann surface associated with the Twist field correlation function $\langle \prod_{j=0}^{2N-1} \mathcal{T}_2(x_j) \rangle$, which we get after a global conformal transformation

$$w = \frac{(z - u_1)(v_N - u_N)}{(v_N - z)(u_N - u_1)}.$$

The partition function $\mathcal{Z}_{N,2}$ may also be written as $\mathcal{Z}_{N,2}^{qu} \mathcal{Z}_{N,2}^{cl}$, where qu and cl stand for quantum and classical part of the Twist field correlation functions discussed in Section 3, these are given by

$$\mathcal{Z}_{N,2}^{qu} \propto \left| \frac{\prod_{j>i=1}^{N}(u_j - u_i)(v_j - v_i)}{\prod_{j,i=1}^{N}(v_i - u_j)} \right|^{\frac{1}{4}} \frac{1}{\sqrt{\det(\mathrm{Img}\Pi)} \left|\Theta(0|\Pi)\right|^2}, \tag{4.7}$$

$$\mathcal{Z}_{N,2}^{cl} \propto \sqrt{\det(\mathrm{Img}\Pi)}\Theta(0|K\Pi)\,\Theta(0|\Pi/K). \tag{4.8}$$

The proportionality constant in $\mathcal{Z}_{N,2}$ is fixed by the small intervals and large distance limit, i.e. $\frac{\ell_i}{d_j} << 1$, for all i, j. In this limit, the reduced density matrix becomes separable and it is just the product of the reduced density matrices for N single intervals. This constant should not be confused with the non-universal constant $c_{N,2}$, which depends on the lattice theory. In the following subsections, we will determine the quantum and classical part of the Twist field correlation function for 2-Rényi CCNR negativity.

4.1 Quantum Part

As discussed in Section 3, we need to evaluate the twist field correlation function eq.(3.3) to find the Rényi CCNR negativity. We also argued that in the case $N > 2$ the associated Riemann surface doesn't have a fixed genus as n varies, as opposed to the $N = 2$ case. This makes the evaluation of the twist field correlation function complicated. The situation is even more complicated for $n > 2$ since the twist fields $\mathcal{T}_{A,n}$ and $\mathcal{T}_{B,n}$ becomes non-Abelian and hence cannot be simultaneously diagonalised. For this reason, in the present work, we will only focus on the $n = 2$ case and hope to come back to the more general case in a later work.

In the $n = 2$ case, we may diagonalise the twist field $\mathcal{T}_A$ and $\mathcal{T}_B$ (we drop the $n = 2$ in the subscript notation for brevity) simultaneously,

$$
\mathcal{T}_A = \begin{bmatrix} 0 & 0 & 0 & 1 \\ 0 & 0 & 1 & 0 \\ 0 & 1 & 0 & 0 \\ 1 & 0 & 0 & 0 \end{bmatrix}, \qquad \mathcal{T}_B = \begin{bmatrix} 0 & 1 & 0 & 0 \\ 1 & 0 & 0 & 0 \\ 0 & 0 & 0 & 1 \\ 0 & 0 & 1 & 0 \end{bmatrix} \tag{4.9}
$$

by the changing the field basis from φ to $\tilde{\varphi}$,

$$
[\tilde{\varphi}] = \frac{1}{2} \begin{bmatrix} -1 & 1 & -1 & 1 \\ 1 & 1 & 1 & 1 \\ -1 & -1 & 1 & 1 \\ 1 & -1 & -1 & 1 \end{bmatrix} [\varphi]. \tag{4.10}
$$

The diagonalised Twist fields are then given by,

$$
\mathcal{T}_A = \begin{bmatrix} -1 & 0 & 0 & 0 \\ 0 & 1 & 0 & 0 \\ 0 & 0 & -1 & 0 \\ 0 & 0 & 0 & 1 \end{bmatrix}, \qquad \mathcal{T}_B = \begin{bmatrix} -1 & 0 & 0 & 0 \\ 0 & 1 & 0 & 0 \\ 0 & 0 & 1 & 0 \\ 0 & 0 & 0 & -1 \end{bmatrix}. \tag{4.11}
$$

In this basis, we'll then need to evaluate the following correlation function,

$$
Z_N \propto \langle \mathcal{T}_{A,1/2}(u_1)\mathcal{T}_{A,1/2}(v_1) \prod_{j=2}^{N} \mathcal{T}_{B,1/2}(u_j)\mathcal{T}_{B,1/2}(v_j)\rangle \langle \prod_{j=2}^{N}\mathcal{T}_{B,1/2}(u_j)\mathcal{T}_{B,1/2}(v_j)\rangle
$$
$$
\langle \mathcal{T}_{A,1/2}(u_1)\mathcal{T}_{A,1/2}(v_1)\rangle, \tag{4.12}
$$

However, such a change of basis will result in non-trivial winding for the field $\tilde{\varphi}$ around the twist fields. This will make the calculation of the classical part complicated and for

this reason, we will calculate the classical part in subsection 4.3 directly from eq.(3.3). The quantum part, however, is independent of the winding and depends upon only the global monodromy of the fields around the twist fields [79], hence it becomes easier to compute it this way.

For the reasons that will become clear later, we use global conformal transformation w to fix the points $u_1 \to -\infty$, $v_1 \to 0$, and $v_N \to 1$,

$$w = \frac{(z - v_1)(v_N - u_1)}{(z - u_1)(v_N - v_1)}, \tag{4.13}$$

and under w we have the following map for the branch points,

$$y_{2j-3} = \frac{(u_j - v_1)(v_N - u_1)}{(u_j - u_1)(v_N - v_1)} \qquad y_{2j-2} = \frac{(v_j - v_1)(v_N - u_1)}{(v_j - u_1)(v_N - v_1)}, \tag{4.14}$$

where $j \in \{1, \dots, N\}$. Under this map, we have the following expression for the twist field correlation function

$$\langle \mathcal{T}_{A,1/2}(u_1) \cdots \mathcal{T}_{B,1/2}(v_N) \rangle = \left(\frac{(v_N - u_1)^{N-1}(v_1 - u_1)^{N-2}}{(v_N - v_1)^{N-1} \prod_{j=2}^{N}(u_j - u_1)(v_j - v_1)} \right)^{\frac{1}{4}}$$
$$\langle \mathcal{T}_{A,1/2}(-\infty) \cdots \mathcal{T}_{B,1/2}(1) \rangle, \tag{4.15}$$

where we have introduced $\mathcal{T}_{A,1/2}(-\infty) = \lim_{w \to -\infty} w^{1/4} \mathcal{T}_{A,1/2}(w)$. The quantum part of the twist field correlation function is known in literature [79–82], see specifically [83] for the present calculations. To compute the quantum part, first, let us consider the Riemann surface corresponding to the twist fields on the right side of the above equation. This surface is parametrised by the curve

$$y^2 = \prod_{i=0}^{2N-2} (w - y_i). \tag{4.16}$$

As discussed in Appendix A to find the period matrix, we introduce a homology basis as shown in Figure 3. We choose the basis of holomorphic differentials of the first kind $\mathrm{d}\mu_j$ to be

$$\mathrm{d}\mu_j(w) = \frac{w^{j-1}}{y} \mathrm{d}w. \tag{4.17}$$

The Riemann period matrix Ω_N, is then determined by using eq.(4.17) in eq.(A.6)-(A.7). We checked that the period matrix Ω_N obtained here is the same as one would obtain in eq.(4.4) using the conventions of Appendix A. The quantum part of the twist field correlation function is given by

$$\langle \mathcal{T}_{1/2}(-\infty) \cdots \mathcal{T}_{1/2}(1) \rangle_{\mathrm{qu}} \propto \left| \frac{\prod_{k>l}^{N}(y_{i_k} - y_{i_l})(y_{j_k} - y_{j_l})}{\prod_{k,l}^{N}(y_{i_k} - y_{j_k})} \right|^{\frac{1}{4}} \frac{1}{\sqrt{\det(\mathrm{Img}\Omega_N)}\Theta[\boldsymbol{e}](0|\Omega_N)^2}, \tag{4.18}$$

where the branch points groups into two disjoint sets $\{y_{i_k}\}$ and $\{y_{j_k}\}$, with each set having N points [84]. Note that we have dropped the subscripts A and B above since the quantum part
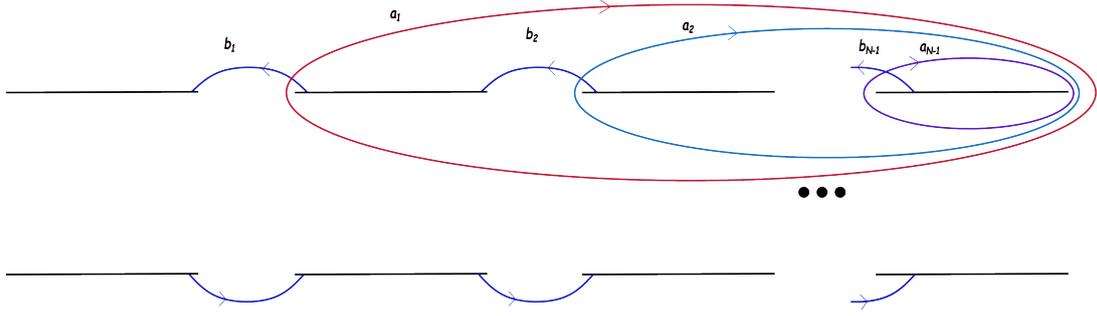
Figure 3. Homology basis for general N: Homology basis for Σ_N is shown above, the horizontal lines represent branch cuts.

is independent of A and B. This grouping depends upon the choice of the characteristics $\boldsymbol{e}$. We set $\boldsymbol{e} = 0$, then one of the sets, say $\{y_{i_k}\}$ is just the collections of branch points that are the zeros of theta function $\Theta(\boldsymbol{\alpha}|\Omega_N)$ under the Abel-Jacobi map $\boldsymbol{\alpha}$ along with the branch point 0. The Abel-Jacobi map is defined from the Riemann surface Σ_N to its Jacobian torus $J(\Sigma_N)$ and is a $(N-1)$ dimensional vector in the present case given by

$$\alpha_j(w) = \int_0^w \mathrm{d}\nu_j(w'). \tag{4.19}$$

The normalised holomorphic differentials $\mathrm{d}\nu_j$ are obtained by using eq.(4.17) in eq.(A.6), using the homology basis given by Figure 3. To determine this grouping, we first note Theta function relation

$$\Theta \begin{bmatrix} \boldsymbol{0} \\ \boldsymbol{0} \end{bmatrix} (\Omega_N \cdot g_1 + g_2 \mid \Omega_N) = e^{-i\pi g_1^t \cdot \Omega_N \cdot g_1 - i2\pi g_1^t \cdot g_2} \Theta \begin{bmatrix} \boldsymbol{g1} \\ \boldsymbol{g2} \end{bmatrix} (0 \mid \Omega). \tag{4.20}$$

The theta function vanishes for all odd characteristics, that is when the characteristics g_1 and g_2 satisfy $4g_1^t \cdot g_2 = 1 \mod 2$. We may thus conclude that $\boldsymbol{\alpha}(y_j) = \Omega_N \cdot g_1 + g_2$ is a zero of theta function if this condition is satisfied. We have

$$(g_1)_i = \frac{1}{2} u(j-i) \text{ for } y_{2j-1}, y_{2j},$$
$$(g_2)_i = \frac{1}{2} (\delta_{1,i} - \delta_{j,i}) \text{ for } y_{2j-1}, y_{2j-2}, \tag{4.21}$$

where $u(x)$ is unit step function and vanishes only for $x < 0$. Therefore we find that the y_{2j} are the zeros of the theta function, and the two sets are given by

$$\{y_{i_k}\} = \{0, y_2, \cdots y_{2N-2}\}, \qquad \{y_{j_k}\} = \{-\infty, y_1, \cdots y_{2N-3}\}. \tag{4.22}$$

Using this in eq.(4.18) and subsequently substituting eq.(4.18) in eq.(4.15) we obtain the following expression for the quantum part,

$$\langle \mathcal{T}_{1/2}(u_1) \cdots \mathcal{T}_{1/2}(v_N) \rangle_{\mathrm{qu}} \propto \left| \frac{\prod_{j>i=1}^N (u_j - u_i)(v_j - v_i)}{\prod_{j,i=1}^N (v_i - u_j)} \right|^{\frac{1}{4}} \frac{1}{\sqrt{\det(\mathrm{Img}\Omega_N)}\Theta(0|\Omega_N)^2}, \tag{4.23}$$
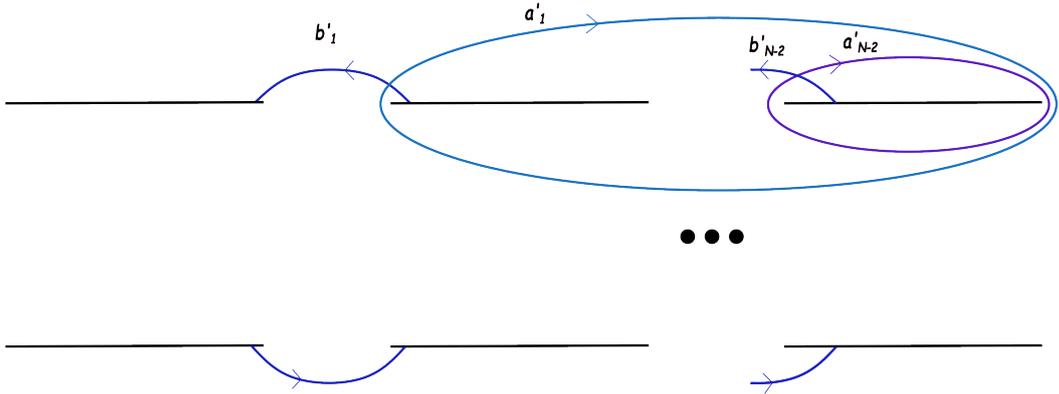
Figure 4. Homology basis for Σ'_{N-1}: Homology basis for Σ'_{N-1} is shown above, the horizontal lines represent branch cuts. The loops may be recognised as $a'_j = a_{j+1}$ and $b'_j = b_{j+1}$, where a, and b are the homology basis on Σ_N.

where we absorbed the algebraic factor of eq.(4.15) in the above expression. We mention that this is the same as the corresponding quantum part in eq.(4.7), as one would expect.

The quantum part of the twist field correlation function $\langle \prod_{j=2}^{N} \mathcal{T}_{B,1/2}(u_j)\mathcal{T}_{B,1/2}(v_j) \rangle$ is similarly evaluated. In this case the relevant Riemann surface Σ'_{N-1} is parametrised by the curve

$$y'^2 = \prod_{j=1}^{2N-2} (w - y_j). \tag{4.24}$$

We choose a holomorphic basis similar to the one shown in Figure 4. The Riemann surface Σ'_{N-1} is just the surface Σ_N with the branch cut $(-\infty, 0)$ removed. The basis of the holomorphic differentials of the first kind may be chosen as

$$\mathrm{d}\mu'_j = \frac{w^{j-1}}{y'}\mathrm{d}w. \tag{4.25}$$

The rest of the calculations follow similarly, and we get the following quantum part for the twist field correlation function

$$\langle \prod_{j=2}^{N} \mathcal{T}_{1/2}(u_j)\mathcal{T}_{1/2}(v_j) \rangle_{\mathrm{qu}} \propto \left| \frac{\prod_{j>i=2}^{N}(u_j - u_i)(v_j - v_i)}{\prod_{j,i=2}^{N}(v_i - u_j)} \right|^{\frac{1}{4}} \frac{1}{\sqrt{\det(\mathrm{Img}\tau_{N-1})}\Theta(0|\tau_{N-1})^2}, \tag{4.26}$$

where τ_{N-1} is the period matrix of the Riemann surface Σ'_{N-1} and it is the same as one would get in eq.(4.4) for the same set of twist fields. The remaining part of eq.(4.12) is simple to evaluate and is given by

$$\langle \mathcal{T}_{1/2}(u_1)\mathcal{T}_{1/2}(v_1) \rangle = \frac{1}{(v_1 - u_1)^{\frac{1}{4}}}. \tag{4.27}$$

We finally obtain the quantum part of eq.(4.12) from eq.(4.23), eq.(4.26), and eq.(4.27) to be

$$Z_N^{\text{qu}} \propto \left| \frac{\prod_{j>i=2}^N (u_j - u_i)(v_j - v_i)}{(v_1 - u_1) \prod_{j,i=2}^N (v_i - u_j)} \right|^{\frac{1}{2}} \left| \frac{\prod_{j=2}^N (u_j - u_1)(v_j - v_1)}{\prod_{j=2}^N (v_j - u_1)(u_j - v_1)} \right|^{\frac{1}{4}} \times$$

$$\frac{1}{\sqrt{\det(\operatorname{Img} \tau_{N-1})} \Theta(0|\tau_{N-1})^2} \frac{1}{\sqrt{\det(\operatorname{Img} \Omega_N)} \Theta(0|\Omega_N)^2},$$
(4.28)

4.2 Classical Part

We will calculate the classical part using a more direct approach, that is by computing the period matrix of the Riemann surface resulting from the Replica trick or the twist field correlation function (3.3). The key observation is that the Riemann surface for $\operatorname{Tr}(RR^\dagger)^2$ is obtained by taking two copies of Σ_N, cutting both of them along the loop a_1, see Figure 3 for the homology basis, and pasting the two copies along this cut, see Figure 5 for illustration.

We mention that this construction is similar to the one which occurs in the evaluation of partition functions for Z_2-orbifold compact boson [81, 85]. While computing the contribution of the twisted sectors to the partition function one introduces a double covering of the torus on which the partition function is computed. Our construction above is the double covering of Σ_N, for the case when the twisted boundary condition is imposed along the loop b_1. We will use this formalism of double covering to compute the period matrix of the desired Riemann surface.

Let us denote by $\hat{\Sigma}_N$ the desired double cover of Σ_N. Let's briefly discuss some properties of $\hat{\Sigma}_N$. First from the Riemann-Hurwitz formula, $\hat{\Sigma}_N$ has a genus $2(N-1)-1 = 2N-3$, as already argued in Section 3. The surface $\hat{\Sigma}_N$ naturally endows a homology basis from Σ_N, as shown in the Figure 5. To describe the construction of this homology basis, we note that there is a conformal automorphism α on $\hat{\Sigma}_N$, satisfying $\alpha \circ \alpha = e$, where e is the identity map. Under this conformal automorphism, the homology basis satisfies the following relations,

$$\alpha \circ \hat{b}_1 = \hat{b}_1 \qquad \alpha \circ \hat{a}_1 = \hat{a}_1,$$
(4.29)

$$\alpha \circ \hat{b}_j = \hat{b}_{2N-3-j} \qquad \alpha \circ \hat{a}_j = \hat{a}_{2N-3-j},$$
(4.30)

where $j \in \{2, \ldots, 2N-3\}$. The basis $\hat{a}_i, \hat{b}_i$, where $i \in \{1, 2 \cdots N-1\}$, are chosen such that under the projection $\hat{\Sigma}_N / \alpha = \Sigma_N$, they project onto a_i, b_i respectively. Note that the loop $\hat{b}_1$ is formed by joining two b_1 loops, as is also seen from Figure 5.

The next step is to find a basis of holomorphic differential of the first kind $d\hat{w}_j$ on $\hat{\Sigma}_N$. The lift of normalised holomorphic differentials $d\nu_j$ on Σ_N gives the first $N-1$ holomorphic differentials of the first kind on $\hat{\Sigma}_N$. The lift of differentials $d\nu_j$ are no longer normalised on $\hat{\Sigma}_N$ since they satisfy

$$\oint_{\hat{a}_1} d\hat{w}_j = \delta_{1,j},$$
(4.31)

$$\oint_{\hat{a}_i} d\hat{w} = \oint_{\hat{a}_{2N-3-i}} d\hat{w} = \delta_{i,j},$$
(4.32)
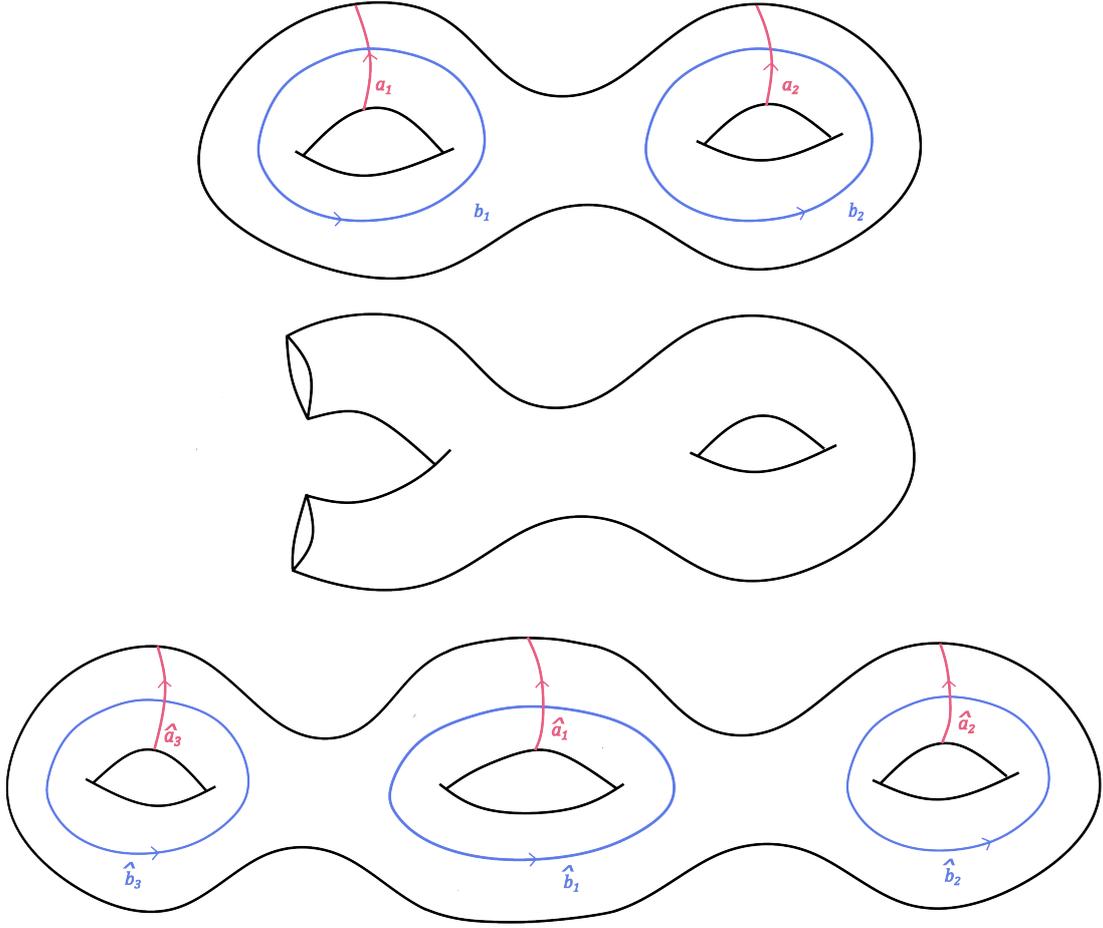
Figure 5. Riemann surface $\hat{\Sigma}_N$: $\hat{\Sigma}_N$ is a double cover of Σ_N, and is constructed by taking two copies of Σ_N, cutting then along the a_1 loop and pasting them together along this cut.

where $i, j \in \{1, 2 \cdots N-1\}$. The remaining $N-2$ holomorphic differentials of the first kind are given by the lift of the Prym differentials on Σ_N, these differentials have a vanishing period around the loops a_1 and b_1, and they are double valued around the loop b_1. The corresponding lift $d\hat{w}_j$ is odd under the conformal automorphism on $\hat{\Sigma}_N$. The differentials $d\hat{w}_j$ satisfy the following relations under the conformal automorphism,

$$\alpha^* \circ d\hat{w}_j = d\hat{w}_j, \qquad j \in \{1, \ldots, N-1\} \tag{4.33}$$

$$\alpha^* \circ d\hat{w}_j = -d\hat{w}_j, \qquad j \in \{N, \ldots, 2N-3\}. \tag{4.34}$$

In the remaining part of this subsection, we will give the construction of $\hat{\Sigma}_N$ from Σ_N following the References [86, 87], and utilize the above formalism to compute the classical part of the twist field correlation function.

To construct the Riemann surface $\hat{\Sigma}$, we make the substitution $\zeta^2 = w$ in eq.(4.24),
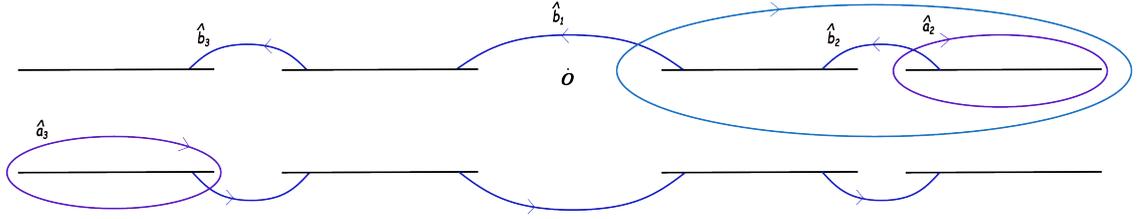
Figure 6. Homology basis on $\hat{\Sigma}_N$: The homology basis $\hat{a}$, and $\hat{b}$ for $N = 3$ is shown in the figure.

and obtain the hyperelliptic curve

$$\hat{y}^2 = \prod_{i=1}^{2N-2} (\zeta - \sqrt{y_i})^{\frac{1}{2}} (\zeta + \sqrt{y_i})^{\frac{1}{2}} . \tag{4.35}$$

The Riemann surface obtained from the branched ζ planes is a model for the surface $\hat{\Sigma}_N$, see [86, 87]. The conformal automorphism α corresponds to a reflection through $\zeta = 0$, followed by an interchange of two ζ sheets, i.e $(\hat{y}, \zeta) \to (-\hat{y}, -\zeta)$. Note that due to the sheet interchange $\zeta = 0$ is not a fixed point, more generally there is no fixed under this conformal automorphism and hence $\hat{\Sigma}_N/\alpha$ is a manifold and not an orbifold. A homology basis for $\hat{\Sigma}_N$ satisfying eq.(4.29)-(4.30) is shown in Figure 6 for $N = 3$ and can be generalised to arbitrary values of N similarly.

We delegate the task of determining the Abelian differentials of the first kind and other necessary quantities to determine the Period matrix to Appendix B. The Period matrix T on $\hat{\Sigma}_N$ is obtained by using eq.(B.6)-(B.7) in eq.(A.6)-(A.7),

$$T_{ij} = \begin{cases} 2\Omega_{1,1} & i = j = 1, \\ \Omega_{i,1} & i \in \{2, \ldots, N-1\}, \\ \Omega_{2N-1-i,1} & i \in \{N, \ldots, 2N-3\}, \\ \Omega_{1,j} & j \in \{2, \ldots, N-1\}, \\ \Omega_{1,2N-1-j} & j \in \{N, \ldots, 2N-3\}, \\ \frac{1}{2}(\Omega_{i,j} + \tau_{i-1,j-1}) & i, j \in \{2, \ldots, N-1\}, \\ \frac{1}{2}(\Omega_{i,2N-1-j} - \tau_{i-1,2N-2-j}) & i \in \{2, \ldots, N-1\}, \ j \in \{N, \ldots, 2N-3\}, \\ \frac{1}{2}(\Omega_{2n-1-i,j} - \tau_{2N-2-i,j-1}) & i \in \{N, \ldots, 2N-3\}, \ j \in \{2, \ldots, N-1\}, \\ \frac{1}{2}(\Omega_{2n-1-i,2n-1-j} + \tau_{2N-2-i,2N-2-j}) & i, j \in \{N, \ldots, 2N-3\}, \end{cases} \tag{4.36}$$

where Ω and τ are the period matrices of Σ_N and Σ'_{N-1} respectively, we have dropped subscript denoting the dependence on N in the notation above for brevity. As an example the Period matrix T for $N = 3$ is given by

$$T = \begin{bmatrix} 2\Omega_{1,1} & \Omega_{1,2} & \Omega_{1,2} \\ \Omega_{2,1} & \frac{1}{2}(\Omega_{2,2} + \tau) & \frac{1}{2}(\Omega_{2,2} - \tau) \\ \Omega_{2,1} & \frac{1}{2}(\Omega_{2,2} - \tau) & \frac{1}{2}(\Omega_{2,2} + \tau) \end{bmatrix} , \tag{4.37}$$

we will use this expression in the next subsection, to compare our results with some numerics. We mention that since Ω and τ in eq.(4.36) are completely imaginary, T is also

completely imaginary. To give the classical part, let us compute the determinant of T. We find,

$$\det(T) = 2\det(\Omega)\det(\tau), \tag{4.38}$$

to see this we will use the row-wise linearity property of the determinants. We split each row of T, except for the first one, into two parts, one containing only Ω terms and the other only τ. We get $(2N-2)^2$ determinants, however most of these vanish since the rows are no longer linearly independent. Consider the determinant where the first $N-1$ rows depend on Ω, and the remaining have τ dependence, it is not that difficult to see that this determinant is $2^{-N+3}\det(\Omega)\det(\tau)$. All the other non-vanishing determinants just correspond to some row interchange between the Ω dependent row and τ dependent row up to a negative sign for the τ dependent row. All such contributions are again $2^{-N+3}\det(\Omega)\det(\tau)$, and there are in total 2^{N-2} of these contributions, and hence we have the result of eq.(4.37).

Finally, the classical part of the twist field correlation function of eq.(3.3) is given by

$$Z_N^{cl} \propto \sqrt{\det(\mathrm{Img}\Omega_\mathrm{N})\det(\mathrm{Img}\tau_\mathrm{N-1})}\,\Theta\left(0|KT\right)\Theta\left(0|T/K\right). \tag{4.39}$$

4.3 2-Rényi CCNR Negativity

To fix the constant of proportionality in $Z_N = Z_N^{cl}Z_N^{qu}$, we consider the limit of faraway intervals, i.e. $\frac{\ell_i}{d_j} << 1$ for all $i,j \in \{1,\dots,N\}$. In this limit, the density matrix ρ will become separable in all intervals, and therefore we would expect the partition function Z_N to be

$$Z_N = \mathcal{Z}_{N,A}^2 \prod_{i=1}^{N-1} \mathcal{Z}_{N,B_i}^2,$$

where $\mathcal{Z}_{N,A}^2$ and $\mathcal{Z}_{N,B_i}^2$ are just the second moment of the single interval density matrix. To see that we get the above decomposition, consider the tensor diagram for the case of two intervals A and B as shown in Figure 7. The extension to arbitrary intervals in the faraway limit is straightforward. It was numerically checked in [60] that in this limit the Theta function in the quantum part goes to unity, similarly, we checked numerically that $\Theta\left(0|T_N\right)$ also goes to unity. Finally, this also implies that the non-universal constant for Z_N is $c_{N,2}^2$, where $c_{N,2}$ is just the non-universal constant for the $n=2$ Rényi entropy for the same set-up. We therefore have the following expression for the total partition function Z_N,

$$Z_N = c_{N,2}^2 \left|\frac{\prod_{j>i=2}^N (u_j-u_i)(v_j-v_i)}{(v_1-u_1)\prod_{j,i=2}^N(v_i-u_j)}\right|^{\frac{1}{2}} \left|\frac{\prod_{j=2}^N (u_j-u_1)(v_j-v_1)}{\prod_{j=2}^N(v_j-u_1)(u_j-v_1)}\right|^{\frac{1}{4}} \tag{4.40}$$
$$\frac{\Theta\left(0|KT_N\right)\Theta\left(0|T_N/K\right)}{\Theta(0|\tau_{N-1})^2\Theta(0|\Omega_N)^2}$$

The 2-Rényi CCNR negativity is just the logarithm of Z_N. As in the case of Rényi Entropy and Rényi negativity, here too we manifestly have an invariance under $K \to 1/K$. The Reflected Rényi entropy is given by

$$S_{2,2}(AA) = -\log\left(\frac{Z_N}{\mathcal{Z}_{N,2}^2}\right), \tag{4.41}$$
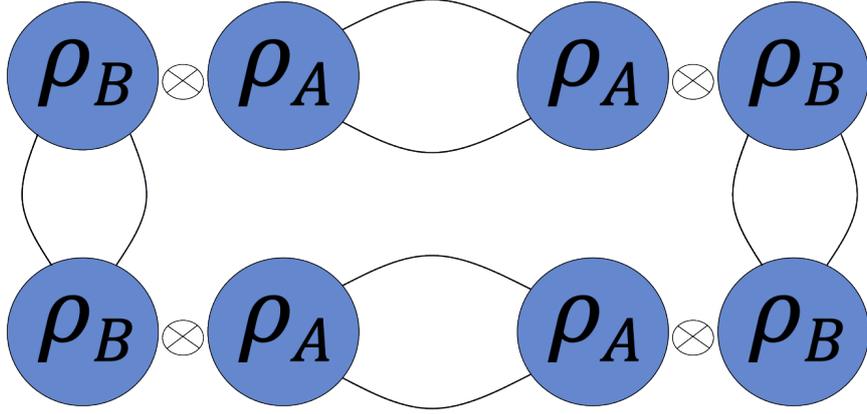
Figure 7. Tensor Diagram for Far distance limit: The density matrix becomes separable in the far distance limit $\rho = \rho_A \otimes \rho_B$, the tensor diagram is shown for $\text{Tr}(RR^\dagger)^2$

.

where $\mathcal{Z}_{N,2}$ is the partition function obtained for 2-Rényi entropy. We see that the ratio $Z_N/\mathcal{Z}_{N,2}^2$ is independent of any non-universal constants and hence the Reflected entropy $S_{2,2}(A\hat{A})$ is a universal quantity.

4.3.1 Recovering the $N = 2$ result

Let us now consider the $N = 2$ case and show that these results match with the known results in the literature. We have from eq.(4.40),

$$Z_2 = c_{2,2}^2 \frac{(u_2 - u_1)^{\frac{1}{4}}(v_2 - v_1)^{\frac{1}{4}}}{(v_2 - u_2)^{\frac{1}{2}}(v_1 - u_1)^{\frac{1}{2}}} \frac{\vartheta_3(2\Omega_2 K)\,\vartheta_3(2\Omega_2/K)}{\vartheta_3(\Omega_2)^2}. \tag{4.42}$$

We will proceed by substituting the moduli Ω_N of the Riemann surface Σ_N with the moduli $2\Omega_2$ of the Riemann surface $\hat{\Sigma}_2$. Using the relation $y^{1/4} = \vartheta_4(\Omega_2)/\vartheta_3(\Omega_2)$, between the moduli Ω_2 and the cross ratio y (see eq.(4.13)-(4.14)), in the theta function relation

$$\vartheta_3^2(\Omega_2) + \vartheta_3^2(\Omega_2) = 2\vartheta_3^2(2\Omega_2),$$

we obtain the following relation between the moduli Ω_2 and $2\Omega_2$,

$$\vartheta_3^2(\Omega_2) = \frac{\vartheta_3^2(2\Omega_2)}{1 + y^{\frac{1}{2}}}. \tag{4.43}$$

Introducing the cross-ration y', where y' is related to y by the following expression,

$$y' = \frac{4y^{\frac{1}{2}}}{(1 + y^{\frac{1}{2}})^2}. \tag{4.44}$$

The cross ratio is related to the moduli $2\Omega_2$ by the following relation,

$$2\Omega_2 = i\frac{F\left(\frac{1}{2}, \frac{1}{2}; 1; y'\right)}{F\left(\frac{1}{2}, \frac{1}{2}; 1; 1 - y'\right)},$$

where F is a hypergeometric function. Note that this is exactly the relation between y and Ω_2 as well. Thus we have a similar relation, $y'^{1/4} = \vartheta_4(2\Omega_2)/\vartheta_3(2\Omega_2)$ and $(1-y')^{1/4} = \vartheta_2(2\Omega_2)/\vartheta_3(2\Omega_2)$, using these relations and as well as eq.(4.44) in eq.(4.42), we obtain the following,

$$\vartheta_3^2(\Omega_2) = \frac{2\left(\vartheta_2\left(2\Omega_2\right)\vartheta_3\left(2\Omega_2\right)\vartheta_4\left(2\Omega_2\right)\right)^{\frac{2}{3}}}{y^{\frac{1}{12}}\left(1-y\right)^{\frac{1}{3}}}. \tag{4.45}$$

Finally substituting this relation in eq.(4.42), we obtain

$$Z_2 = \frac{\tilde{c}_2}{\left(\ell_1\ell_2(v_2-v_1)(v_2-u_1)(u_2-v_1)(u_2-u_1)\right)^{\frac{1}{6}}} \frac{\vartheta_3\left(2\Omega_2 K\right)\vartheta_3\left(2\Omega_2/K\right)}{\left(\vartheta_2\left(2\Omega_2\right)\vartheta_3\left(2\Omega_2\right)\vartheta_4\left(2\Omega_2\right)\right)^{\frac{2}{3}}},$$

where ℓ_1, and ℓ_2 are lengths of the intervals and we absorbed any constants into the non-universal constant $\tilde{c}_2$. This is just the result for $n = 2$ Rényi CCNR entropy obtained in [74].

4.3.2 Dirac Fermions and Numerical checks

The 2-Rényi CCNR negativity for the Dirac fermion may be similarly obtained. It is however known that the partition function of the Dirac fermion matches with that of the self-dual compact boson when the Riemann period matrix Ω is completely imaginary [61], this is indeed the case in the present calculations. Hence the twist field correlation for Dirac fermion is given by

$$Z_N = c_{N,2}^2 \left|\frac{\prod_{j>i=2}^{N}(u_j-u_i)(v_j-v_i)}{(v_1-u_1)\prod_{j,i=2}^{N}(v_i-u_j)}\right|^{\frac{1}{2}} \left|\frac{\prod_{j=2}^{N}(u_j-u_1)(v_j-v_1)}{\prod_{j=2}^{N}(v_j-u_1)(u_j-v_1)}\right|^{\frac{1}{4}}$$
$$\frac{\Theta\left(0|T_N\right)^2}{\Theta(0|\tau_{N-1})^2\Theta(0|\Omega_N)^2}. \tag{4.46}$$

We mention that the self-dual compact boson is not dual to the Dirac fermion, the known duality is between the Z_2-gauged modular invariant Dirac fermion and the compact boson at Bose-Fermi duality radius. The Reflected entropy is given by

$$S_{2,2} = -\log\left(\left|\frac{\prod_{j=2}^{N}(u_j-u_1)(v_j-v_1)}{\prod_{j=2}^{N}(v_j-u_1)(u_j-v_1)}\right|^{-\frac{1}{4}} \frac{\Theta\left(0|T_N\right)^2}{\Theta(0|\tau_{N-1})^2\Theta(0|\Omega_N)^2}\right). \tag{4.47}$$

This result is matched against the tight-binding model for the case of three disjoint intervals, see Figures 8-9 for the plots. The numerical model is given in the Appendix C. Since this ratio is universal there are no fitting parameters in these plots. We see from these plots that there is a very good match between the numerical results and the analytical predictions.

4.4 Different Realignment

We may also study the entanglement of some other interval, instead of A, with the rest of the intervals. In this case, we define the re-alignment matrix with respect to the desired interval. Let us generalise our techniques to this scenario as well. It is rather straightforward
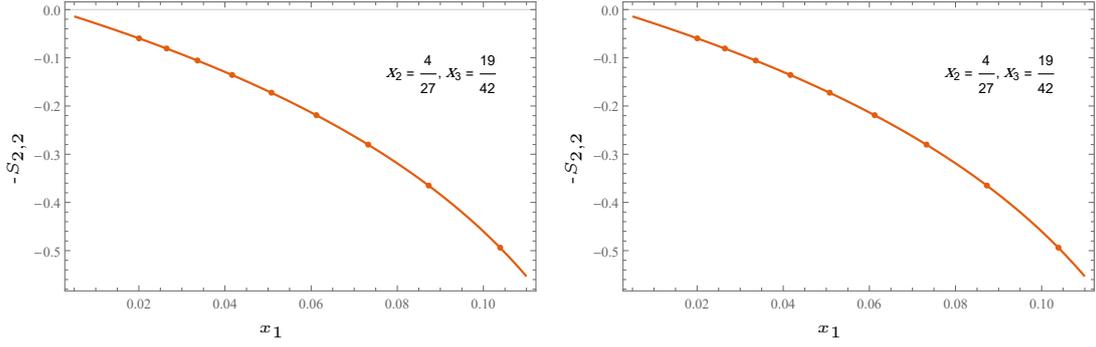
Figure 8. Reflected Entropy Plot for 3 Disjoint intervals: $-S_{2,2}$ is plotted against the cross-ratio x_1, with x_2 and x_3 fixed, see eq.(4.3). The continuous lines are analytical plots for Dirac Fermions while plot points are numerical evaluations for the tight-binding model.
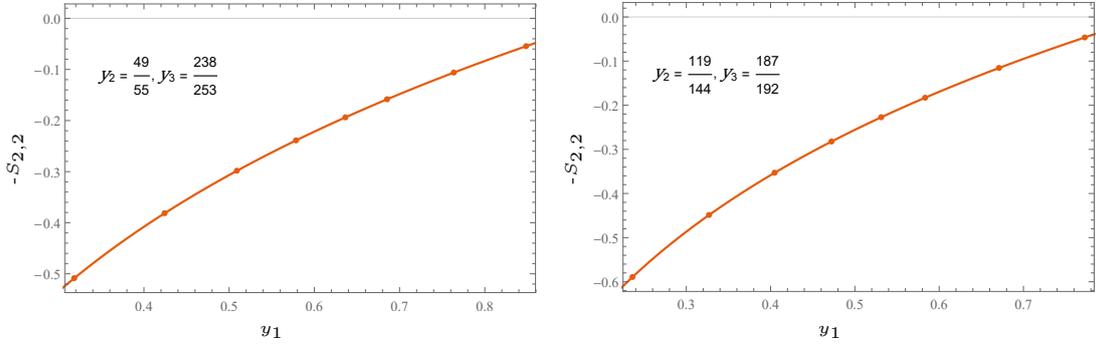
Figure 9. Reflected Entropy Plot for three disjoint intervals: $-S_{2,2}$ is plotted against the cross-ratio y_1, with y_2 and y_3 fixed, see eq.(4.14). The continuous lines are analytical plots for Dirac Fermions while plot points are numerical evaluations for the tight-binding model.

to do so. Let us consider the re-alignment with respect to the second interval as an example. We introduce the map $\tilde{w}$, mapping $u_2 \to -\infty$, $v_2 \to 0$, and $v_1 \to 1$, we have

$$\tilde{w} = \frac{(z - v_2)(u_2 - v_1)}{(z - u_2)(v_2 - v_1)}.\tag{4.48}$$

The remaining branch points have the following mappings,

$$\tilde{y}_{2j-1} = \frac{(u_{j+2} - v_2)(u_2 - v_1)}{(u_{j+2} - u_2)(v_2 - v_1)}, \qquad \tilde{y}_{2j} = \frac{(v_{j+2} - v_2)(u_2 - v_1)}{(v_{j+2} - u_2)(v_2 - v_1)},\tag{4.49}$$

where $j \in \{1, 2, \ldots, N-3\}$ and $u_1 \to \tilde{y}_{2N-3}$. The branch points lie on the real line of the $\tilde{w}$ plane and have the following order, $0 < \tilde{y}_1 < \tilde{y}_2 \ldots < \tilde{y}_{2N-3} < 1$. We then make a similar choice of the homology basis on the cut- surface as in Figure 6. The remaining calculations follows exactly as in Subsections 4.3-4.4, with y_i replaced with $\tilde{y}_i$. Notice that this is in general a different homology basis on the cut-z surface, and with this choice, as is easily seen on the $\tilde{w}$ surface, one of the a loops encircles only the second interval. So we are just
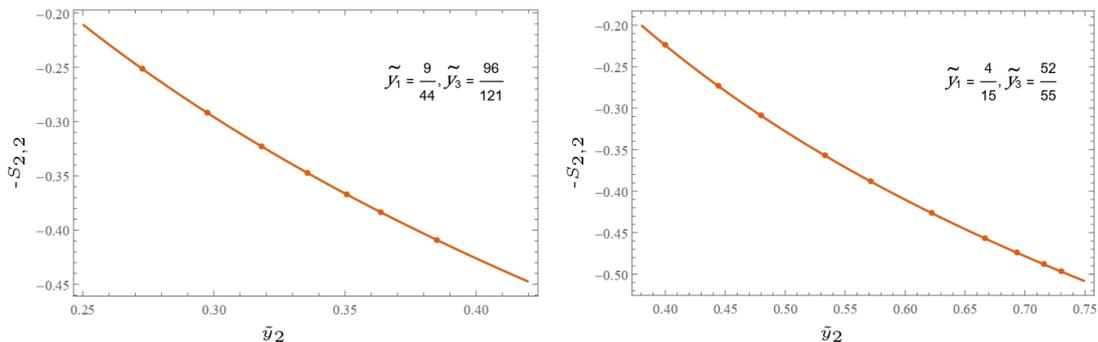
Figure 10. Reflected Entropy Plot for Re-alignment with respect to the second interval (3 interval case): $-S_{2,2}$ is plotted against the cross-ratio $\tilde{y}_2$, with $\tilde{y}_1$ and $\tilde{y}_3$ fixed, see eq.(4.49). The continuous lines are analytical plots for Dirac Fermions while plot points are numerical evaluations for the tight-binding model.

considering a double cover of Σ_N for the case where we have twisted boundary condition along the b loop intersecting this a loop.

We have plotted the Reflected entropy for three intervals with the above construction in Figure 10. Here too we have plotted analytical results for the Dirac fermion against the numerical results of the tight-binding model, see Appendix C. We mention again that we don't have any free parameters in these plots and similar to earlier plots we have a very good match between the two results.

5 Conclusion

In this work, we considered N disjoint intervals and studied the entanglement between a single interval and the union of remaining disjoint intervals. We evaluated the 2-Rényi CCNR (computable cross norm) negativity of compact boson at arbitrary compactification radius for multiple disjoint intervals.

We employed the Replica trick and Twist fields methods to compute the 2-Rényi CCNR negativity. The correlation function of the relevant Twist-fields can written as a product of a quantum part and a classical part. The quantum part was determined by diagonalizing the Twist fields and calculating the quantum component of the correlation functions for the diagonalized Twist fields. The classical part was evaluated directly by computing the Riemann period matrix of the associated Riemann surface $\hat{\Sigma}$. The 2-Rényi CCNR negativity is just the logarithm of this Twist-field correlation function. The expression for 2-Rényi CCNR negativity was given in terms of the period matrices of three Riemann surfaces. One of these surfaces was $\hat{\Sigma}$, the second was the Riemann surface for 2-Rényi entropy of N-disjoint intervals and the last one was the Riemann surface for 2-Rényi entropy of $(N-1)$-disjoint intervals compromising one of the subsystems. We then obtained the Reflected entropy related to the 2-Rényi CCNR negativity. These Reflected entropies are universal quantities, that is we don't need a non-universal constant to compare the CFT results with the lattice models. We also extended our results to massless Dirac fermions.

Finally, we checked our results against the tight-binding model and found a very good agreement between the analytical and numerical results.

There are several future directions of research worth pursuing. It will be interesting to extend these results to all integer values of the Rényi index. Since the Riemann surfaces associated with these calculations do not possess a Z_n-symmetry, as opposed to Rényi entropy and Rényi negativity, it would be very interesting to see the properties of Rényi CCNR negativities for multiple-disjoint interval settings. Another research direction would be to compute the (m, n)-Rényi CCNR negativity, introduced in [75], for the compact boson CFT as similar features will also be present in these calculations even for two disjoint interval settings. Finally, the symmetry resolution of CCNR-negativity for disjoint intervals is still an open problem for compact boson. The symmetry-resolved CCNR negativity of fermions and bosons have been studied in [75] for adjacent intervals and for massless Dirac fermions it has been studied in [76] for two disjoint intervals.

A   Riemann Surfaces

In this appendix, we review some concepts in the theory of Riemann surface relevant to the present work. We refer the reader to [84, 88–90] for a detailed review of Riemann surfaces. Specifically, we introduce homology basis, holomorphic differentials(also referred to as Abelian differentials) of the first kind and the Riemann period matrix for a given Riemann surface. In our discussions we will consider the Riemann surface $\tilde{\Sigma}_N$, parametrised by the following curve

$$u^2 = \prod_{j=0}^{2N-2} (z - x_j)^{\frac{1}{2}},$$

this is the Riemann surface that we consider in Section 4 for $n = 2$ Rényi Entropy of multiple disjoint intervals, see discussion around eq.(4.6). These results can be easily generalised to other cases and we will refer to these results for our main computations. It follows from eq.(4.3), $x_0 = 0 < x_1 < x_2 \cdots < x_{2N-2} = 1$. We consider the homology basis given by the a and b loops, that is the basis of non-contractible loops on the Riemann surface, as shown in Figure 11 for the specific case of $N = 3$. The basis, irrespective of the Riemann surface, satisfies the following intersection rules

$$a_i \circ a_j = b_i \circ b_j = 0 \tag{A.1}$$

$$a_i \circ b_j = -b_i \circ a_j = \delta_{i,j} \tag{A.2}$$

The a_i loops run counter-clockwise and encircle the first i intervals of the branch cuts on the principle Riemann sheet. The b_j loops run from the $(j + 1)^{\text{th}}$ cut to the jth cut on the principle sheet and passes through the jth cut and meets itself after passing through the $(j + 1)^{\text{th}}$ on the second sheet. This choice of a and b loops indeed satisfies the relations (A.1)-(A.2).

Let us now pick the basis of the Abelian differentials of the first kind dw_i, where $i \in \{1, 2 \cdots N - 1\}$, to be the conventional one. They are given by

$$dw_i(z) = \frac{z^{i-1}}{u(z)} dz. \tag{A.3}$$
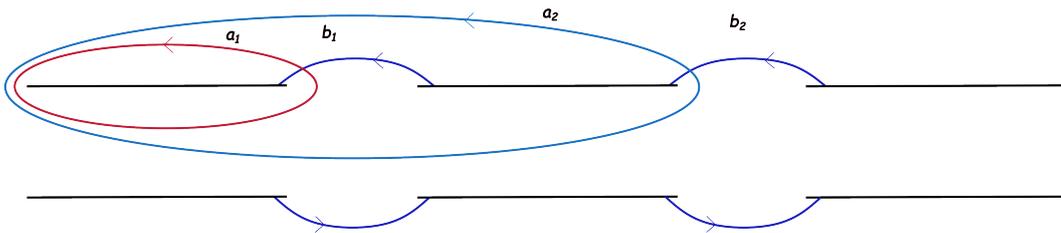
Figure 11. Homology basis (N=3): Homology basis for Σ_3 is shown above, the horizontal lines represent branch cuts.

These Abelian differentials define the following $(N-1) \times (N-1)$ matrices A and B,

$$A_{i,j} = \oint_{a_j} \mathrm{d}w_i(z), \qquad B_{i,j} = \oint_{b_j} \mathrm{d}w_i(z). \tag{A.4}$$

These contour integrals may be computed using the following set of integrals,

$$\mathcal{I}^i_{x_{2j},x_{2j+1}} = \int_{x_{2j}}^{x_{2j+1}} \mathrm{d}w_i(z), \tag{A.5}$$

which are just Lauricella functions [60]. We can now introduce normalised holomorphic differentials $\mathrm{d}\nu_i(z)$,

$$\mathrm{d}\nu_i(z) = A^{-1}_{i,j} \mathrm{d}w_j(z), \tag{A.6}$$

so that they satisfy $\oint_{a_i} \mathrm{d}\nu_j(z) = \delta_{i,j}$. Finally, using the normalised holomorphic differentials we define the Riemann period matrix Π,

$$\Pi_{i,j} = \oint_{b_j} \mathrm{d}z\nu_i(z). \tag{A.7}$$

Note that the period matrix is independent of the choice of the basis of the Abelian differentials of the first kind and are given in the homology basis a and b. As mentioned in the main text, Π is a symmetric matrix with a positive definite imaginary part. In fact in the present case, that is for Riemann surfaces given by eq.(4.6), the real part of the period matrix vanishes and hence it is purely imaginary.

B   Riemann Surface $\hat{\Sigma}_N$

In this Appendix, we find the Abelian differentials of the first kind on the Riemann surface $\hat{\Sigma}_N$. We also give the matrices A and B by computing the contour integral of these differentials along the loops $\hat{a}$ and $\hat{b}$

As mentioned in subsection 4.2, the first $(N-1)$ of the Abelian differentials of the first kind are constructed by lifting the normalised holomorphic differentials $\mathrm{d}\nu_j$ on Σ_N, we substitute $w = \zeta^2$ in the normalised differentials to obtain

$$\mathrm{d}w_i = \left(A_N^{(-1)}\right)_{ij} \zeta^{2(j-1)} \prod_{k=1}^{2N-2} (\zeta - \sqrt{y_k})^{-\frac{1}{2}} (\zeta - \sqrt{y_i})^{-\frac{1}{2}} \mathrm{d}\zeta, \tag{B.1}$$

where we have absorbed any constant into the definition of $\mathrm{d}w_i$, and the matrix A_N is evaluated on Σ_N as discussed in Appendix A, specifically see eq.(A.4). The Prym differentials may be constructed from the Abelian differentials of the first kind on Σ'_{N-1}, given by eq.(4.24)-(4.26), for reference we reproduce them here

$$\mathrm{d}\mu'_j = w^{j-1} \prod_{i=1}^{2N-2} (w - y_k)^{-\frac{1}{2}}.$$

These differentials have a zero period around the loops a_1, and b_1 on Σ_N. To see this we note hat loop a_1 is contractible on Σ'_{N-1}, and loop b_1 encloses only one branch point, infact b_1 is not a closed loop on Σ'_{N-1}. Finally, we also note that $\mathrm{d}\mu'_j$ are odd when taken around the loop b_1 on Σ_N. This implies that the normalised holomorphic differentials on Σ'_{N-1} are the Prym differentials on Σ_N. We therefore obtain the remaining Abelian differentials of the first kind by similarly lifting the Prym differentials, we have

$$\mathrm{d}w_{2N-3-i} = \left(A_{N-1}^{\prime(-1)} \right)_{ij} \zeta^{2j-1} \prod_{k=1}^{2N-2} (\zeta - \sqrt{y_k})^{-\frac{1}{2}} (\zeta - \sqrt{y_k})^{-\frac{1}{2}} \mathrm{d}\zeta, \tag{B.2}$$

where $I \in \{1, \ldots, N-2\}$ and as before we have absorbed any constant into $\mathrm{d}w_{2N-3-j}$. The matrix A'_{N-1} is just the A matrix of eq.(A.4) on Σ'_{N-1}.

As mentioned in the main text, the conformal automorphism on $\hat{\Sigma}_N$ is a reflection through $\zeta = 0$ followed by a sheet interchange. Now, to evaluate the contour integrals of $\mathrm{d}w_j$ around the homology basis $\hat{a}$, and $\hat{b}$, see Figure 6, we must carefully pick the correct branches for the integrand. We choose the principle branch for the integrand to be below the cuts for all the branch cuts to the left of the origin on the first sheet. Now we may evaluate the matrices A, and B by using the following integrals,

$$\begin{aligned} I^j_{\sqrt{y_i}, \sqrt{y_{j+i}}} &= \int_{\sqrt{y_i}}^{\sqrt{y_{i+1}}} \mathrm{d}\zeta \zeta^{2(j-1)} \prod_{k=1}^{2N-2} (\zeta - \sqrt{y_k})^{-\frac{1}{2}} (\zeta - \sqrt{y_k})^{-\frac{1}{2}} \\ &= \frac{1}{2} \int_{y_i}^{y_{i+1}} \mathrm{d}z z^{j-1} \prod_{k=0}^{2N-1} (z - y_k)^{-\frac{1}{2}}, \end{aligned} \tag{B.3}$$

where $j \in \{1, 2 \cdots N-1\}$. Similarly for the remaining $\mathrm{d}w_j$ we have,

$$I^{2N-3-j}_{\sqrt{y_i}, \sqrt{y_{j+i}}} = \frac{1}{2} \int_{y_i}^{y_{i+1}} \mathrm{d}z z^{j-1} \prod_{k=1}^{2N-1} (z - y_k)^{-\frac{1}{2}}. \tag{B.4}$$

We also note that under the conformal automorphism α, the differentials $\mathrm{d}w_j$ are even when $j \in \{1, \ldots, N-1\}$ and odd when $j \in \{N, \ldots, 2N-3\}$, this in accordance with eq.(4.33)-(4.34). The matrix B maybe written in terms of the Riemann period matrices Ω_N and τ_{N-1} of Riemann surfaces Σ_N and Σ'_{N-1} respectively. These matrices are found to be

$$A_{ij} = \begin{cases} \frac{1}{2} & j = i; \ i \in \{1, \ldots, N-1\} \\ \frac{1}{2} & j = 2N-1-i; \ i \in \{2, \ldots, N-1\} \\ \frac{1}{2} & j = i - N + 2; \ i \in \{N, \cdots, 2N-3\} \\ -\frac{1}{2} & j = 3N-3-i; \ i \in \{N, \ldots, 2N-3\} \\ 0 & \text{otherwise,} \end{cases} \tag{B.5}$$

$$
B_{ij} = \begin{cases} \Omega_{i,1} & i \in \{1, \ldots, N-1\} \\ \frac{1}{2}\Omega_{i,j} & i,j \in \{2, \ldots, N-1\} \\ \frac{1}{2}\Omega_{i,2N-1-j} & i \in \{2, \ldots, N-1\},\ j \in \{N, \ldots, 2N-3\} \\ \frac{1}{2}\tau_{i-N+1,j-1} & i \in \{N, \ldots, 2N-3\},\ j \in \{2, \ldots, N-1\} \\ -\frac{1}{2}\tau_{i-N+1,2N-2-j} & i \in \{N, \ldots, 2N-3\},\ j \in \{N, \ldots, 2N-3\} \\ 0 & \text{otherwise.} \end{cases} , \tag{B.6}
$$

where we have dropped the subscript on Ω and τ above for brevity. Note we did not normalise the differentials $d\hat{w}$ according to eq.(4.31)-(4.32) and so we get factors of $\frac{1}{2}$ in eq.(B.5)-(B.6), but this is really of no consequence. The inverse of matrix A is given by,

$$
A^{(-1)}{}_{ij} = \begin{cases} 2 & i = j = 1 \\ 1 & i = j;\ i \in \{1, \ldots, N-1\} \\ 1 & i = 2N-1-j;\ j \in \{2, \ldots, N-1\} \\ 1 & i = j-N+2;\ j \in \{N, \ldots, 2N-3\} \\ -1 & i = 3N-3-j;\ j \in \{N, \ldots, 2N-3\} \\ 0 & \text{otherwise.} \end{cases} \tag{B.7}
$$

We have used these results in the main text to obtain the period matrix T for $\hat{\Sigma}_N$, see eq.(4.35).

C   Numerical Model

In this section, we give the numerical evaluation of Rényi CCNR negativity and Reflected entropies for the tight-binding model. The results for Reflected entropies are used in the plots of Figures 8, 9 and 10. This method for Reflected Entropy was first developed in [91, 92] and later was generalised to Rényi CCNR Negativities and (m, n)-Rényi Reflected entropies in [75] for both fermions and bosons.

Tight-binding model has the Hamiltonian $H = -\sum_i \hat{c}_{i+1}^\dagger \hat{c}_i + \hat{c}_i^\dagger \hat{c}_{i+1}$. The fermionic operators $\hat{c}_i$ satisfies the following commutation relations $\{\hat{c}_i, \hat{c}_j^\dagger\} = \delta_{i,j}$. The correlation matrix $C_{ij} = \left\langle \hat{c}_i^\dagger \hat{c}_j \right\rangle$ for the tight binding model is given by

$$
C_{ij} = \frac{\sin\left((i-j)\pi/2\right)}{(i-j)\pi}. \tag{C.1}
$$

The reduced density matrix for the subsystem $A \cup B$ may be given by the diagonalised Gaussian state,

$$
\rho_{AB} = \prod_k \frac{e^{-\epsilon_k a_k^\dagger a_k}}{1 + e^{-\epsilon_k}}, \tag{C.2}
$$

where the fermion operators a_k are related to the operators c_i, where $i \in \{A \cup B\}$, via an unitary transformation. The spectrum ϵ_k of the Gaussian state is related to the eigenvalues $\frac{1+\nu_k}{2}$ of the correlation matrix C_{AB} via [93],

$$
\frac{1}{1 + e^{\epsilon_k}} = \frac{1 + \nu_k}{2}, \tag{C.3}
$$

where C_{AB} is the restriction of the correlation matrix C to the subsystem $A \cup B$. The Rényi entropies for the reduced density matrix ρ_{AB} is then given by

$$S_n(AB) = \frac{1}{1-n} \operatorname{Tr} \log(C_{AB}^n + (1-C_{AB})^n). \tag{C.4}$$

To generalise this formalism to (m,n)-Reflected entropies and CCNR Rényi negativities, we consider the Choi-Jamiolkowski isomorphism for ρ_{AB}^m,

$$|\Omega_m\rangle = \frac{1}{\sqrt{\operatorname{Tr}\rho_{AB}^m}} \prod_k \frac{\left(1 + e^{-\frac{m\epsilon_k}{2}} a_k^\dagger \tilde{a}_k^\dagger\right)}{(1 + e^{-\epsilon_k})^{\frac{m}{2}}} |0\rangle|\tilde{0}\rangle. \tag{C.5}$$

where the operators a_k and $\tilde{a}_k$ belong to the either copy of the hilbert space $\mathcal{H}_{AB}$. The correlation matrix for these operators is given by

$$\langle\Omega_m| \begin{pmatrix} a_k^\dagger \\ \tilde{a}_k \end{pmatrix} \left(a_{k'} \ \tilde{a}_{k'}^\dagger \right) |\Omega_m\rangle = \delta_{kk'} \frac{(1+e^{\epsilon_k})^m}{1+e^{m\epsilon_k}} \begin{bmatrix} \frac{1}{(1+e^{-\epsilon_k})^m} & \frac{e^{-\frac{m\epsilon_k}{2}}}{(1+e^{-\epsilon_k})^m} \\ \frac{e^{-\frac{m\epsilon_k}{2}}}{(1+e^{-\epsilon_k})^m} & \frac{e^{-m\epsilon_k}}{(1+e^{-\epsilon_k})^m} \end{bmatrix}. \tag{C.6}$$

Let's denote this correlation matrix by $\tilde{C}^{(m)}$, in the (doubled) spatial basis this correlation matrix is given by,

$$\tilde{C}^{(m)} = \frac{1}{C_{AB}^m + (1-C_{AB})^m} \begin{bmatrix} C_{AB}^m & C_{AB}^{\frac{m}{2}}(1-C_{AB})^{\frac{m}{2}} \\ C_{AB}^{\frac{m}{2}}(1-C_{AB})^{\frac{m}{2}} & (1-C_{AB})^m \end{bmatrix}. \tag{C.7}$$

We now assume that the Reflected reduced density matrix ρ_{AA} is also given by a diagonalised Gaussian state,

$$\rho_{AA} = \prod_k \frac{e^{-\tilde{\epsilon}_k b_k^\dagger b_k}}{1 + e^{-\tilde{\epsilon}_k}}, \tag{C.8}$$

where the operators b_k are related to the operators c_i and $\tilde{c}_i^\dagger$, where $i \in \{A\}$, by a unitary transformation. Then from eq.(C.2)-(C.4), we conclude that the (m,n)-Reflected Rényi entropy is given by,

$$S_{m,n} = \frac{1}{1-n} \operatorname{Tr} \log\left(\left(\tilde{C}_A^{(m)}\right)^n + \left(1 - \tilde{C}_A^{(m)}\right)^n\right), \tag{C.9}$$

where $\tilde{C}_A^{(m)}$ is the restriction of $\tilde{C}^{(m)}$ to the degrees of freedom in the doubled subspace A. We are interested in the case $m = n = 2$ for the numerical plots in Figures 8, 9 and 10. Finally, the CCNR negativity is given by using the relation in eq.(2.7).

Acknowledgments

References

[1] Shinsei Ryu and Tadashi Takayanagi. Holographic derivation of entanglement entropy from AdS/CFT. *Phys. Rev. Lett.*, 96:181602, 2006.

[2] Tatsuma Nishioka, Shinsei Ryu, and Tadashi Takayanagi. Holographic Entanglement Entropy: An Overview. *J. Phys. A*, 42:504008, 2009.

[3] Sergey N. Solodukhin. Entanglement entropy of black holes. *Living Rev. Rel.*, 14:8, 2011.

[4] Michael A. Nielsen and Isaac L. Chuang. *Quantum Computation and Quantum Information: 10th Anniversary Edition*. Cambridge University Press, 2010.

[5] Luigi Amico, Rosario Fazio, Andreas Osterloh, and Vlatko Vedral. Entanglement in many-body systems. *Rev. Mod. Phys.*, 80:517–576, 2008.

[6] A. Osterloh, Luigi Amico, G. Falci, and Rosario Fazio. Scaling of entanglement close to a quantum phase transition. *Nature*, 416(6881):608–610, 2002.

[7] G. Vidal, J. I. Latorre, E. Rico, and A. Kitaev. Entanglement in quantum critical phenomena. *Phys. Rev. Lett.*, 90:227902, 2003.

[8] Pasquale Calabrese and John L. Cardy. Entanglement entropy and quantum field theory. *J. Stat. Mech.*, 0406:P06002, 2004.

[9] Asher Peres. Separability criterion for density matrices. *Phys. Rev. Lett.*, 77:1413–1415, 1996.

[10] Michal Horodecki, Pawel Horodecki, and Ryszard Horodecki. On the necessary and sufficient conditions for separability of mixed quantum states. *Phys. Lett. A*, 223:1, 1996.

[11] Oliver Rudolph. Some properties of the computable cross-norm criterion for separability. *Phys. Rev. A*, 67(3):032312, 2003.

[12] K. Chen and L. A. Wu. A matrix realignment method for recognizing entanglement. *Quant. Inf. Comput.*, 3(3):193–202, 2003.

[13] Oliver Rudolph. Further Results on the Cross Norm Criterion for Separability. *Quant. Inf. Proc.*, 4(3):219–239, 2005.

[14] Christoph Holzhey, Finn Larsen, and Frank Wilczek. Geometric and renormalized entropy in conformal field theory. *Nucl. Phys. B*, 424:443–467, 1994.

[15] Pasquale Calabrese and John Cardy. Entanglement entropy and conformal field theory. *J. Phys. A*, 42:504005, 2009.

[16] Eduardo Fradkin and Joel E. Moore. Entanglement entropy of 2D conformal quantum critical points: hearing the shape of a quantum drum. *Phys. Rev. Lett.*, 97:050404, 2006.

[17] John Cardy and Erik Tonni. Entanglement hamiltonians in two-dimensional conformal field theory. *J. Stat. Mech.*, 1612(12):123103, 2016.

[18] Francisco Castilho Alcaraz, Miguel Ibanez Berganza, and German Sierra. Entanglement of low-energy excitations in Conformal Field Theory. *Phys. Rev. Lett.*, 106:201601, 2011.

[19] Benjamin Hsu, Michael Mulligan, Eduardo Fradkin, and Eun-Ah Kim. Universal entanglement entropy in 2D conformal quantum critical points. *Phys. Rev. B*, 79:115421, 2009.

[20] Pasquale Calabrese, John Cardy, and Erik Tonni. Finite temperature entanglement negativity in conformal field theory. *J. Phys. A*, 48(1):015006, 2015.

[21] Hassan Shapourian, Ken Shiozaki, and Shinsei Ryu. Partial time-reversal transformation and entanglement negativity in fermionic systems. *Phys. Rev. B*, 95(16):165101, 2017.

[22] Pasquale Calabrese and John L. Cardy. Evolution of entanglement entropy in one-dimensional systems. *J. Stat. Mech.*, 0504:P04010, 2005.

[23] Pasquale Calabrese and John Cardy. Entanglement and correlation functions following a local quench: a conformal field theory approach. *J. Stat. Mech.*, 0710(10):P10004, 2007.

[24] Xueda Wen, Po-Yao Chang, and Shinsei Ryu. Entanglement negativity after a local quantum quench in conformal field theories. *Phys. Rev. B*, 92(7):075109, 2015.

[25] Andrea Coser, Erik Tonni, and Pasquale Calabrese. Entanglement negativity after a global quantum quench. *J. Stat. Mech.*, 1412(12):P12017, 2014.

[26] Marianne Hoogeveen and Benjamin Doyon. Entanglement negativity and entropy in non-equilibrium conformal field theory. *Nucl. Phys. B*, 898:78–112, 2015.

[27] J. L. Cardy, O. A. Castro-Alvaredo, and B. Doyon. Form factors of branch-point twist fields in quantum integrable models and entanglement entropy. *J. Statist. Phys.*, 130:129–168, 2008.

[28] Benjamin Doyon. Bi-partite entanglement entropy in massive two-dimensional quantum field theory. *Phys. Rev. Lett.*, 102:031602, 2009.

[29] Olalla A. Castro-Alvaredo and Benjamin Doyon. Bi-partite entanglement entropy in massive 1+1-dimensional quantum field theories. *J. Phys. A*, 42:504006, 2009.

[30] Davide Bianchini, Olalla A. Castro-Alvaredo, and Benjamin Doyon. Entanglement Entropy of Non-Unitary Integrable Quantum Field Theory. *Nucl. Phys. B*, 896:835–880, 2015.

[31] Olivier Blondeau-Fournier, Olalla A. Castro-Alvaredo, and Benjamin Doyon. Universal scaling of the logarithmic negativity in massive quantum field theory. *J. Phys. A*, 49(12):125401, 2016.

[32] Olalla A. Castro-Alvaredo, Cecilia De Fazio, Benjamin Doyon, and István M. Szécsényi. Entanglement Content of Quasiparticle Excitations. *Phys. Rev. Lett.*, 121(17):170602, 2018.

[33] Olalla A. Castro-Alvaredo and Benjamin Doyon. Bi-partite entanglement entropy in massive QFT with a boundary: The Ising model. *J. Statist. Phys.*, 134:105–145, 2009.

[34] Huan-Qiang Zhou, Thomas Barthel, John Ove Fjærestad, and Ulrich Schollwöck. Entanglement and boundary critical phenomena. *Physical Review A—Atomic, Molecular, and Optical Physics*, 74(5):050305, 2006.

[35] Eyal Cornfeld and Eran Sela. Entanglement entropy and boundary renormalization group flow: Exact results in the Ising universality class. *Phys. Rev. B*, 96(7):075153, 2017.

[36] Benoit Estienne, Yacine Ikhlef, Andrei Rotaru, and Erik Tonni. Entanglement entropies of an interval for the massless scalar field in the presence of a boundary. *JHEP*, 05:236, 2024.

[37] Luca Capizzi, Sara Murciano, and Pasquale Calabrese. Rényi entropy and negativity for massless Dirac fermions at conformal interfaces and junctions. *JHEP*, 08:171, 2022.

[38] Luca Capizzi, Sara Murciano, and Pasquale Calabrese. Rényi entropy and negativity for massless complex boson at conformal interfaces and junctions. *JHEP*, 11:105, 2022.

[39] Michael Gutperle and John D. Miller. Entanglement entropy at CFT junctions. *Phys. Rev. D*, 95(10):106008, 2017.

[40] Kantaro Ohmori and Yuji Tachikawa. Physics at the entangling surface. *J. Stat. Mech.*, 1504:P04010, 2015.

[41] David Rogerson, Frank Pollmann, and Ananda Roy. Entanglement entropy and negativity in the Ising model with defects. *JHEP*, 06:165, 2022.

[42] Luca Capizzi and Viktor Eisler. Entanglement evolution after a global quench across a conformal defect. *SciPost Phys.*, 14(4):070, 2023.

[43] Olalla A. Castro-Alvaredo and Lucía Santamaría-Sanz. Symmetry Resolved Measures in Quantum Field Theory: a Short Review. 3 2024.

[44] Moshe Goldstein and Eran Sela. Symmetry-resolved entanglement in many-body systems. *Phys. Rev. Lett.*, 120(20):200602, 2018.

[45] Eyal Cornfeld, Moshe Goldstein, and Eran Sela. Imbalance entanglement: Symmetry decomposition of negativity. *Phys. Rev. A*, 98(3):032302, 2018.

[46] J. C. Xavier, F. C. Alcaraz, and G. Sierra. Equipartition of the entanglement entropy. *Phys. Rev. B*, 98(4):041106, 2018.

[47] Sara Murciano, Riccarda Bonsignori, and Pasquale Calabrese. Symmetry decomposition of negativity of massless free fermions. *SciPost Phys.*, 10(5):111, 2021.

[48] Nick G. Jones. Symmetry-Resolved Entanglement Entropy in Critical Free-Fermion Chains. *J. Statist. Phys.*, 188(3):28, 2022.

[49] Sara Murciano, Giuseppe Di Giulio, and Pasquale Calabrese. Entanglement and symmetry resolution in two dimensional free quantum field theories. *JHEP*, 08:073, 2020.

[50] Alessandro Foligno, Sara Murciano, and Pasquale Calabrese. Entanglement resolution of free Dirac fermions on a torus. *JHEP*, 03:096, 2023.

[51] Luca Capizzi, Dávid X. Horváth, Pasquale Calabrese, and Olalla A. Castro-Alvaredo. Entanglement of the 3-state Potts model via form factor bootstrap: total and symmetry resolved entropies. *JHEP*, 05:113, 2022.

[52] David X. Horvath, Luca Capizzi, and Pasquale Calabrese. U(1) symmetry resolved entanglement in free 1+1 dimensional field theories via form factor bootstrap. *JHEP*, 05:197, 2021.

[53] Gilles Parez, Riccarda Bonsignori, and Pasquale Calabrese. Quasiparticle dynamics of symmetry-resolved entanglement after a quench: Examples of conformal field theories and free fermions. *Phys. Rev. B*, 103(4):L041104, 2021.

[54] Giuseppe Di Giulio, René Meyer, Christian Northe, Henri Scheppach, and Suting Zhao. On the boundary conformal field theory approach to symmetry-resolved entanglement. *SciPost Phys. Core*, 6:049, 2023.

[55] Yuya Kusuki, Sara Murciano, Hirosi Ooguri, and Sridip Pal. Symmetry-resolved entanglement entropy, spectra & boundary conformal field theory. *JHEP*, 11:216, 2023.

[56] Pasquale Calabrese, Jérôme Dubail, and Sara Murciano. Symmetry-resolved entanglement entropy in Wess-Zumino-Witten models. *JHEP*, 10:067, 2021.

[57] Shunsuke Furukawa, Vincent Pasquier, and Jun'ichi Shiraishi. Mutual Information and Compactification Radius in a c=1 Critical Phase in One Dimension. *Phys. Rev. Lett.*, 102:170602, 2009.

[58] Pasquale Calabrese, John Cardy, and Erik Tonni. Entanglement entropy of two disjoint intervals in conformal field theory. *J. Stat. Mech.*, 0911:P11001, 2009.

[59] Pasquale Calabrese, John Cardy, and Erik Tonni. Entanglement entropy of two disjoint intervals in conformal field theory II. *J. Stat. Mech.*, 1101:P01021, 2011.

[60] Andrea Coser, Luca Tagliacozzo, and Erik Tonni. On Rényi entropies of disjoint intervals in conformal field theory. *J. Stat. Mech.*, 1401:P01008, 2014.

[61] Matthew Headrick, Albion Lawrence, and Matthew Roberts. Bose-Fermi duality and entanglement entropies. *J. Stat. Mech.*, 1302:P02022, 2013.

[62] Andrea Coser, Erik Tonni, and Pasquale Calabrese. Spin structures and entanglement of two disjoint intervals in conformal field theories. *J. Stat. Mech.*, 1605(5):053109, 2016.

[63] Vincenzo Alba, Luca Tagliacozzo, and Pasquale Calabrese. Entanglement entropy of two disjoint intervals in c=1 theories. *J. Stat. Mech.*, 1106:P06012, 2011.

[64] M. A. Rajabpour and F. Gliozzi. Entanglement Entropy of Two Disjoint Intervals from Fusion Algebra of Twist Fields. *J. Stat. Mech.*, 1202:P02016, 2012.

[65] Paola Ruggiero, Erik Tonni, and Pasquale Calabrese. Entanglement entropy of two disjoint intervals and the recursion formula for conformal blocks. *J. Stat. Mech.*, 1811(11):113101, 2018.

[66] Filiberto Ares, Pasquale Calabrese, Giuseppe Di Giulio, and Sara Murciano. Multi-charged moments of two intervals in conformal field theory. *JHEP*, 09:051, 2022.

[67] Himanshu Gaur and Urjit A. Yajnik. Multi-charged moments and symmetry-resolved Rényi entropy of free compact boson for multiple disjoint intervals. *JHEP*, 01:042, 2024.

[68] Pasquale Calabrese, John Cardy, and Erik Tonni. Entanglement negativity in quantum field theory. *Phys. Rev. Lett.*, 109:130502, 2012.

[69] Pasquale Calabrese, John Cardy, and Erik Tonni. Entanglement negativity in extended systems: A field theoretical approach. *J. Stat. Mech.*, 1302:P02008, 2013.

[70] Andrea Coser, Erik Tonni, and Pasquale Calabrese. Towards the entanglement negativity of two disjoint intervals for a one dimensional free fermion. *J. Stat. Mech.*, 1603(3):033116, 2016.

[71] Cristiano De Nobili, Andrea Coser, and Erik Tonni. Entanglement entropy and negativity of disjoint intervals in CFT: Some numerical extrapolations. *J. Stat. Mech.*, 1506(6):P06021, 2015.

[72] Hui-Huang Chen. Charged Rényi negativity of massless free bosons. *JHEP*, 02:117, 2022.

[73] Himanshu Gaur and Urjit A. Yajnik. Charge imbalance resolved Rényi negativity for free compact boson: Two disjoint interval case. *JHEP*, 02:118, 2023.

[74] Chao Yin and Zhenhuan Liu. Universal Entanglement and Correlation Measure in Two-Dimensional Conformal Field Theories. *Phys. Rev. Lett.*, 130(13):131601, 2023.

[75] Clément Berthiere and Gilles Parez. Reflected entropy and computable cross-norm negativity: Free theories and symmetry resolution. *Phys. Rev. D*, 108(5):054508, 2023.

[76] Andrea Bruno, Filiberto Ares, Sara Murciano, and Pasquale Calabrese. Symmetry resolution of the computable cross-norm negativity of two disjoint intervals in the massless Dirac field theory. *JHEP*, 02:009, 2024.

[77] Souvik Dutta and Thomas Faulkner. A canonical purification for the entanglement wedge cross-section. *JHEP*, 03:178, 2021.

[78] Thierry Giamarchi. *Quantum Physics in One Dimension*. Oxford University Press, 12 2003.

[79] Lance J. Dixon, Daniel Friedan, Emil J. Martinec, and Stephen H. Shenker. The Conformal Field Theory of Orbifolds. *Nucl. Phys. B*, 282:13–73, 1987.

[80] Erik P. Verlinde and Herman L. Verlinde. Chiral Bosonization, Determinants and the String Partition Function. *Nucl. Phys. B*, 288:357, 1987.

[81] Robbert Dijkgraaf, Erik P. Verlinde, and Herman L. Verlinde. C = 1 Conformal Field Theories on Riemann Surfaces. *Commun. Math. Phys.*, 115:649–690, 1988.

[82] Luis Alvarez-Gaume, Gregory W. Moore, and Cumrun Vafa. Theta Functions, Modular Invariance and Strings. *Commun. Math. Phys.*, 106:1–40, 1986.

[83] A. B. Zamolodchikov. Conformal Scalar Field on the Hyperelliptic Curve and Critical Ashkin-teller Multipoint Correlation Functions. *Nucl. Phys. B*, 285:481–503, 1987.

[84] David Mumford, Madhav Nori, and Peter Norman. *Tata lectures on theta III*, volume 43. Springer, 2007.

[85] Kei Miki. Vacuum Amplitudes Without Twist Fields for $Z(N)$ Orbifold and Correlation Functions of Twist Fields for $Z(2)$ Orbifold. *Phys. Lett. B*, 191:127–134, 1987.

[86] Harry E Rauch and Hershel M Farkas. Theta constants of two kinds on a compact riemann surface of genus 2. *Journal d'Analyse Mathématique*, 23(1):381–407, 1970.

[87] Hershel M Farkas and Harry E Rauch. Period relations of schottky type on riemann surfaces. *Annals of Mathematics*, 92(3):434–461, 1970.

[88] John David Fay. *Theta functions on Riemann surfaces*, volume 352. Springer, 2006.

[89] Luis Alvarez-Gaume, C. Gomez, and C. Reina. NEW METHODS IN STRING THEORY. 6 1987.

[90] Luis Alvarez-Gaume and Philip C. Nelson. RIEMANN SURFACES AND STRING THEORIES. In *4th Trieste Spring School on Supersymmetry, Supergravity, Superstrings: (followed by 3 day Workshop)*, 12 1986.

[91] Pablo Bueno and Horacio Casini. Reflected entropy, symmetries and free fermions. *JHEP*, 05:103, 2020.

[92] Pablo Bueno and Horacio Casini. Reflected entropy for free scalars. *JHEP*, 11:148, 2020.

[93] Ingo Peschel. Calculation of reduced density matrices from correlation functions. *J. Phys. A*, 36(14):L205, 2003.